remote sensing

MDPI

Article

Daily Mapping of 30 m LAI and NDVI for Grape Yield Prediction in California Vineyards

Liang Sun [1,*], Feng Gao [1], Martha C. Anderson [1], William P. Kustas [1], Maria M. Alsina [2], Luis Sanchez [2], Brent Sams [2], Lynn McKee [1], Wayne Dulaney [1], William A. White [1], Joseph G. Alfieri [1], John H. Prueger [3], Forrest Melton [4,5] and Kirk Post [4]

1 U. S. Department of Agriculture, Agricultural Research Service, Hydrology and Remote Sensing Laboratory, Beltsville, MD 20705, USA; feng.gao@ars.usda.gov (F.G.); martha.anderson@ars.usda.gov (M.C.A.); bill.kustas@ars.usda.gov (W.P.K.); Lynn.McKee@ars.usda.gov (L.M.); Wayne.Dulaney@ars.usda.gov (W.D.); Alex.White@ars.usda.gov (W.A.W.); Joe.Alfieri@ars.usda.gov (J.G.A.)

2 E & J Gallo Winery Viticulture Research, Modesto, CA 95354, USA; MariadelMar.Alsina@ejgallo.com (M.M.A.); Luis.Sanchez@ejgallo.com (L.S.); Brent.Sams@ejgallo.com (B.S.)

3 USDA-ARS, National Laboratory for Agriculture and the Environment, Ames, IA 50011, USA; John.Prueger@ars.usda.gov

4 California State University, Monterey Bay, School of Natural Resources, Seaside, CA 93933, USA; Forrest.S.Melton@nasa.gov (F.M.); kpost@csumb.edu (K.P.)

5 NASA Ames Research Center, Moffett Field, CA 94035, USA

* Correspondence: sunliang001@gmail.com or liang.sun@ars.usda.gov; Tel.: +1-301-504-8554

Academic Editors: Assefa M. Melesse, Alfredo R. Huete, Clement Atzberger and Prasad S. Thenkabail
Received: 28 November 2016; Accepted: 23 March 2017; Published: 28 March 2017

Abstract: Wine grape quality and quantity are affected by vine growing conditions during critical phenological stages. Field observations of vine growth stages are too sparse to fully capture the spatial variability of vine conditions. In addition, traditional grape yield prediction methods are time consuming and require large amount grape samples. Remote sensing data provide detailed spatial and temporal information regarding vine development that is useful for vineyard management. In this study, Landsat surface reflectance products from 2013 and 2014 were used to map satellite-based Normalized Difference Vegetation Index (NDVI) and leaf area index (LAI) over two *Vitis vinifera* L. cv. Pinot Noir vineyards in California, USA. The spatial correlation between grape yield maps and the interpolated daily time series (LAI and NDVI) was quantified. NDVI and LAI were found to have similar performance as a predictor of spatial yield variability, providing peak correlations of 0.8 at specific times during the growing season, and the timing of this peak correlation differed for the two years of study. In addition, correlations with maximum and seasonal-cumulative vegetation indices were also evaluated, and showed slightly lower correlations with the observed yield maps. Finally, the within-season grape yield predictability was examined using a simple strategy in which the relationship between grape yield and vegetation indices were calibrated with limited ground measurements. This strategy has a strong potential to improve the accuracy and efficiency of yield estimation in comparison with traditional approaches used in the wine grape growing industry.

Keywords: wine grape; satellite remote sensing; NDVI; LAI; yield; field-scale

1. Introduction

Over 99 percent of grapes grown commercially in the United States come from California, which accounts for nearly 90 percent of American wine production valued at approximately $6 billion from 918,000 acres of vineyards in 2015 [1]. The ability to accurately and efficiently monitor vine development and estimate grape yields within season will have significant benefit to the wine industry

such as efficient harvest organization, regional pricing negotiations, and tank space allocation for vintage and marketing strategies [2]. An over-cropped vine has an insufficient exposed leaf area relative to the retained fruit weight, leading to delayed ripening, lower fruit quality and an eventual decrease in vine size, limiting future yield potential and reducing cold hardiness of both buds and wood. An under-cropped vine has an excess of exposed leaf area relative to the weight of the retained fruit crop. It will be more prone to fungal diseases and will also have reduced fruit quality [3].

Viticulturists have developed several systems for estimating yield, but all are based on sampling: (a) the number of grape-bearing vines per acre; (b) the number of grape clusters per vine, and most notably; and (c) cluster weight [2,4,5]. The sample size and distribution is determined by row and vine spacing, which means that the spatial variability should be considered. Growers must determine whether, when and how much fruit they should remove at thinning time. Accordingly, daily monitoring of vineyard conditions is required for optimal grape management, but ground-based measurements are not likely to be representative of whole-field conditions and are costly to install and maintain, especially for large scale and distributed production systems.

Remotely sensed data offer strong advantages over other monitoring techniques by providing a timely, synoptic, and up-to-date overview of actual crop growing conditions over large areas at multiple stages during the growing season. It has been found that there are strong relationships between satellite-based vegetation indices such as NDVI and vine development across vineyards [6–8]. In addition, remote sensing data have also been used to extract grapevine shape/size [9], to predict grape phenolics and color [10], and to discriminate different varieties within vineyards [11,12].

In addition to NDVI, a direct biophysical parameter for monitoring vine conditions is leaf area index (LAI) which provides specific physical information regarding canopy functioning; therefore, high-quality LAI retrieved from remotely sensed data is a valuable asset [13,14]. Many approaches have been developed to estimate LAI using Landsat. These approaches can be classified into two basic categories: (1) using empirical relationships between LAI and vegetation indices [15,16]; and (2) through the inversion of a physical radiative transfer (RT) model [17]. The inversion of a RT model could be implemented by seeking the solution with minimum cost iteratively, using a lookup table (LUT) method [13] or neural network (NN) algorithm [18]. Although the NDVI approach is simple, it is usually sensitive to soil and atmospheric conditions as well as measurement geometries and spatial resolutions, and thus no unique relationship between LAI and NDVI is universally applicable [19]. The conventional RT model inversion with an iterative process is both time consuming and hard to extend to regional and global scales, although it is more universal and may have a better accuracy. In this study we evaluate a reference-based approach to mapping LAI with Landsat developed by Gao et al. [20], which uses Landsat surface reflectance (SR) maps to downscale Moderate Resolution Imaging Spectroradiometer (MODIS) LAI products. This method has been successfully incorporated into the DisALEXI ET model [21] to map energy fluxes at 30 m resolution [22–24] and to provide a MODIS-consistent LAI data product from Landsat imagery.

The objective of this paper is to evaluate the relationships between grape yields and Landsat-derived LAI and NDVI time-series at field scale (30 m) for improving grape yield prediction through combining the limited field sampling with remote sensing data. While previous studies have shown the correlation between crop yields and satellite-based vegetation indices (VI) [6,25–27], vineyard yield estimation is more complex due to intensive management of the grape and vine development to maximize production goals, which may vary from year to year based on climate, economics, and market demand. For example, the vineyard manager might remove some clusters early in the season in order to drive quality in the remaining clusters [28]. Although it is difficult to establish a universal model to make year-to-year prediction of at-harvest yield using remote-sensing based indices, it is still very important for the grape growers to predict yield before harvest by the sampling method as described above.

This study focuses on the spatial variability of grape yields for 2013 and 2014 achieved in two adjacent Pinot Noir vineyards located in the Central Valley of California, USA. The spatial correlations

between yield, and NDVI and LAI were evaluated and analyzed. Based on the findings, a simple grape yield prediction strategy, combing satellite based VI and limited within-field samples, is proposed for improving grape yield estimation before harvest.

2. Methods

2.1. Landsat-Resolution LAI Estimation

Landsat data (30 m) provide a unique opportunity to characterize crop conditions and water stress at field or sub-field scales. In addition to spatial resolution requirements, high temporal resolution is also needed to capture the dynamics of crop growth through time, especially at critical growth stages [29]. While a single Landsat satellite has a relatively long revisit cycle of 16 days, at present we have access to both Landsat 7 and 8 data, which together can provide acquisitions at one location as often as every 8 days, depending on cloud cover.

A regression tree method is used for retrieving Landsat LAI using homogeneous and high quality MODIS LAI as a reference [20]. The MODIS LAI product (500 m) has been validated and analyzed with independent field measurements [30,31]. In this approach, Landsat surface reflectances are aggregated to match coarse-resolution MODIS data, extracted from MODIS LAI products over the Landsat scene of interest. Only high-quality MODIS LAI samples retrieved from the main algorithm (based on RT model) are selected based on the product quality flags. The selected MODIS LAI samples are further screened to exclude pixels with high sub-pixel variability in Landsat reflectance, thus ensuring that only homogeneous MODIS pixels are used in the training process. As LAI has a nonlinear relation to spectral reflectance and NDVI, a multi-variant regression tree approach (cubist by RuleQuest) is used in the processing. LAI and surface reflectance samples at MODIS pixel resolution are used to train the MODIS resolution model. The derived regression trees are finally applied to the Landsat surface reflectances at their native 30-m resolution to produce Landsat-scale LAI maps.

2.2. TIMESAT

The TIMESAT program package was designed primarily for smoothing and filtering time-series of satellite data [32,33]. TIMESAT has been used successfully to analyze time-series VI data from the Advanced Very High Resolution Radiometer (AVHRR) [33,34] and from MODIS [35–37]. In this study, we used an adaptive Savitzky–Golay (SG) filtering function supplied by TIMESAT to interpolate Landsat-retrieved NDVI and LAI maps from clear days to daily timesteps.

2.3. Yield Correlation Analyses

Gridded yield data collected within-field (as described in Section 3.4) were aggregated to 30 m resolution consistent with the Landsat data grids. The spatial correlation between yield VI was quantified using the Pearson correlation coefficient (R). To identify an optimal window during the growing season where an index is the best correlated to the yield at harvest, the daily time-series indices were accumulated and summarized over different intervals (from 1-day to 120-day) prior to computation of correlations. A 1-day interval gives a daily comparison, while a 120-day interval corresponds to almost the entire growing season, which starts from late March/early April and ends at harvest at the end of August/early September. The nominal growing season was defined as Day of Year (DOY) 91 (1 April) to 273 (30 September).

2.4. Grape Yield Prediction Model

Using the satellite index from the time interval identified by the methods in Section 2.3 as providing the optimal correlation with yields, a simple operational yield prediction approach is proposed and evaluated. First, the location of the maximum and the minimum satellite index pixel values from the optimal correlation date are located. At these locations within the field, a sampling box is defined where the vegetation index is measured in situ on the optimal correlation date. Then, grape

weight and cluster areal density at the same sampling box can be measured in situ before harvest. Finally, a linear function is fitted based on the index and grape weights measured from the field (only two samples), and used to estimate production field-wide based on the satellite index image on the optimal correlation date. Compared to traditional methods which have to choose enough samples to represent the large area, the grape yield prediction model proposed here only needs two samples, which will greatly improve the grape yield prediction efficiency and reduce sampling costs. In this study, the maximum and minimum index and corresponding yield (grape weight and density) were extracted from the images representing the samples measured from fields, and then used to test the model.

3. Study Area and Data

3.1. Study Area

The Central Valley of California has abundant sunshine, large day-and-night temperature differences, and an evaporative demand ranging from 889 to 1270 mm of water during the growing season, making it a primary wine grape producing area in the USA. Our study area extended over two *Vitis vinifera* L. cv. Pinot Noir vineyards located near Lodi in central California as Figure 1 shown [22,38]. The northern field (Site 1) has an area of about 35 ha and is a more mature vineyard (9–10 years old in 2016), while the southern field (Site 2) is smaller in size, at about 21 ha and 6–7 years old. The height of the vines ranges between 2 and 2.5 m, with row spacing approximately 3.35 m and an average vine spacing along the row of 1.52 m. Both fields have an east-west row orientation. Variations in soil texture, vine age and health result in a fairly wide range in vine biomass across the two fields. The vines typically budburst in mid-late March and grow through August before the grapes are harvested in early September. When winter rains and soil moisture are adequate, a grass cover crop flourishes early in the growing season in the inter-row until becoming senescent starting in early May, which is typically the beginning of the dry season. The cover crop helps to remove excess soil moisture from winter rains before vine budbreak. Drip irrigation typically commences sometime early in June and is continued until harvest if necessary. Decisions to begin irrigation in a field for a season are typically triggered by different factors, including visual assessment of canopy water stress, spot measurements of leaf water potential with gas pressure chambers, soil moisture, and upcoming weather conditions.

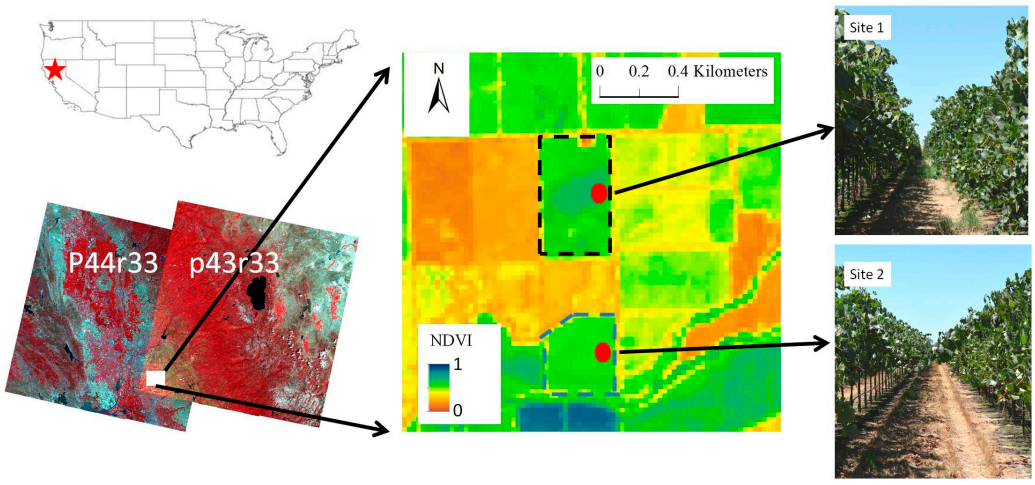

Figure 1. Study area. The upper field confined by the dashed black line in the middle image is the north vineyard (Site 1) and the lower field confined by the dashed blue line is the south vineyard (Site 2). The North vineyard is planted with 9–10-year-old Pinot Noir vines, and the South vineyard is planted with 6–7-year-old Pinot Noir vines. The red circles correspond to the LAI measurement locations.

3.2. Ground Measurement Data

Two selected Pinot Noir vineyards were part of the Grape Remote sensing Atmospheric Profiling and Evapotranspiration eXperiment (GRAPEX) [22,38], which aims to combine in-situ and remotely-sensed data to investigate the effects of canopy structure and row orientation of energy and moisture exchange processes within and above the vine canopy. A critical component of GRAPEX has been to work closely and collaboratively with scientist at Ernest & Julio Gallo Winery to ensure that both the experimental data and models can address critical operational needs, including improving grape quality, yield estimation and irrigation strategies. GRAPEX measurements include ground, airborne and satellite remote sensing, surface energy balance, turbulence and mean profile measurements of wind temperature and water vapor focusing on above, below and between vine canopy, surface and sub-surface soil moisture, along with ground-based biophysical measurements of LAI and leaf-level conductance, transpiration and photosynthesis. Several intensive observation periods (IOPs) were conducted in 2013–2014 to collect biophysical measurements of the vine canopy during different phenological stages. The IOPs were scheduled to be coincident with Landsat 8 overpass times to provide validation of satellite-derived variables. The date and the number of measurements of the IOPs were listed in Table 1.

Table 1. LAI measurement information.

Year	DOY	IOPs	Instrument	Sensor	Path/Row	Overpass
2013	162	IOP1	Li-Cor LAI-2000	L7	044033	162
	212	IOP2	Li-Cor LAI-2000	L8	043033	211
	219	IOP3	Li-Cor LAI-2000	L8	044033	218
	226	IOP4	Li-Cor LAI-2000	L8	043033	227
2014	181	IOP1	Li-Cor LAI-2200	L7	044033	181
	221	IOP2	Li-Cor LAI-2200	L8	044033	221
	269	IOP3	Li-Cor LAI-2200	-	-	-

The LAI measurements were made using a Li-Cor LAI-2000 (or 2200) instrument along several transects, collecting four below-canopy samples and one above-canopy reading to obtain an estimate of the effective LAI of the vine/inter-row system. The four below-canopy samples were collected: (1) under the vine and directly in-line with the vine row; (2) one-quarter of the distance from the row and the adjacent row of vines; (3) half way between rows in the center of the inter-row; and (4) three-quarters of the distance from the row to the adjacent row. Measurements were made with and without including the inter-row cover crop, which had a very minor impact on the LAI measurements for the field IOPs in June through August. Vines grow in the early spring and rapidly expand in leaf area mid to late May, and the observed LAI increased throughout the season until harvest in early September.

3.3. Landsat and MODIS Data Products

Landsat 7 (L7) and Landsat 8 (L8) atmospherically corrected surface reflectance products over the study area for the period from 2013–2014 were directly downloaded from the USGS EarthExplorer website [39]. A total of 166 scenes were processed (see Figure 2). The study area lies in the overlap between path 43/row 33 and path 44/row 33, and this fortuitous location—along with low cloud cover during growing season—makes it possible to collect sufficient clear Landsat scenes to support interpolation to daily maps. Although Landsat 7 has striped gaps in all but the center of each scene missing, due to the SLC (Scan Line Corrector) failure that occurred since May of 2003, these gaps can be filled by interpolating Landsat 7 and 8 data using the TIMESAT program.

MODIS 4-day composite LAI products (MCD15A3, Collection 5; Myneni, 2014) for 2013–2014 over the study area were used. In contrast to the Terra-MODIS (MOD15A2), Aqua-MODIS (MYD15A2), and the combined Terra and Aqua MODIS (MCD15A2) versions of the 8-day LAI products, the 4-day

composited MODIS LAI product (MCD15A3) has increased temporal frequency and helps to monitor phenology and associated rapid changes (that occur within less than a week), especially during transition periods (green-up and senescence). One MODIS tile (h08v05) was selected to cover both Landsat scenes. The LAI-reflectance samples from the entire Landsat scene over the entire year were used to train and build the regression trees. The regression trees were then applied to Landsat resolution reflectance to generate Landsat-scale LAI as Section 2.1 described.

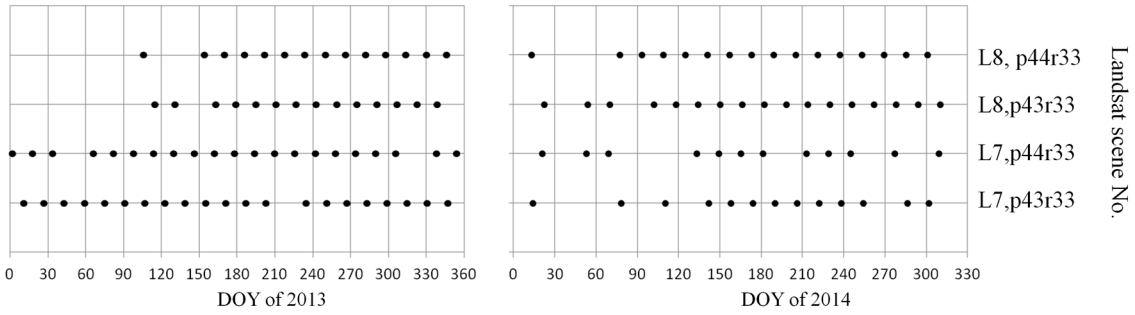

Figure 2. Landsat 7 and 8 scenes collected over the study area from 2013–2014. Each dot represents a Landsat acquisition date.

3.4. Grape Yields

Yield maps for 2013 and 2014 harvest in both fields were provided by E & J Gallo Winery. Advanced Technology Viticulture (ATV, Joslin, Australia) yield monitor systems were installed on three self-propelled, over-the-row, trunk-shaking mechanical GH9000 AIM harvesters (Agricultural Industrial Manufacturing, Lodi, CA, USA). Yield monitors consist of a combined GPS receiver and antenna, as well as a specialized grape weighing and data recording system consisting of a load cell weight bridge, belt speed sensor, and data logger. Harvest data were transferred into a cleanup script written in R Studio software (RStudio Inc., Boston, MA, USA) to convert mass flow units into tons per hectare, eliminate outliers, and normalize data across harvesters. Yield data more than three standard deviations from the mean were removed to reduce scatter, which usually results in removal of less than 5% of the total yield data. After cleanup, the data were interpolated to 3 × 3 m resolution grids, and then aggregated up to the 30-m Landsat grid resolution.

4. Results and Analysis

4.1. Landsat NDVI and LAI

Figure 3 shows 30-m resolution maps of NDVI and estimated LAI over the GRAPEX fields on three selected days, with corresponding ground pictures taken from Site 1. Day 93, 173, and 253 separately correspond to the start, middle, and end of the growing season. LAI and NDVI have similar distributions, and the spatial pattern of the vegetation conditions within the fields and surrounding areas are clearly evident, supporting the hypothesis that field-scale management practices can be effectively informed by Landsat-scale resolution imagery. The maps for DOY 93 (early in the growing season) primarily reflect green biomass in the grass cover crop (see photo from Site 1). On this day, LAI in the north field is about 1.5–1.8 and NDVI is about 0.5–0.6, while the south field has LAI values that range from 1.6–2.5 and NDVI values of 0.5–0.7. DOY 173 is around the time of peak vine biomass, with NDVI around 0.6–0.7 and LAI of 1.7–2.2 over the vineyards. DOY 253 (10 September) occurred before grape harvest, which is at the end of September, so the vegetation cover on this day is much lower than that on DOY 173. NDVI ranged 0.5–0.6 and LAI ranged 1.3–1.5 over GRAPEX vineyard fields on DOY 253. The lower vine LAI on this day is also reflected in the ground photograph in Figure 3.

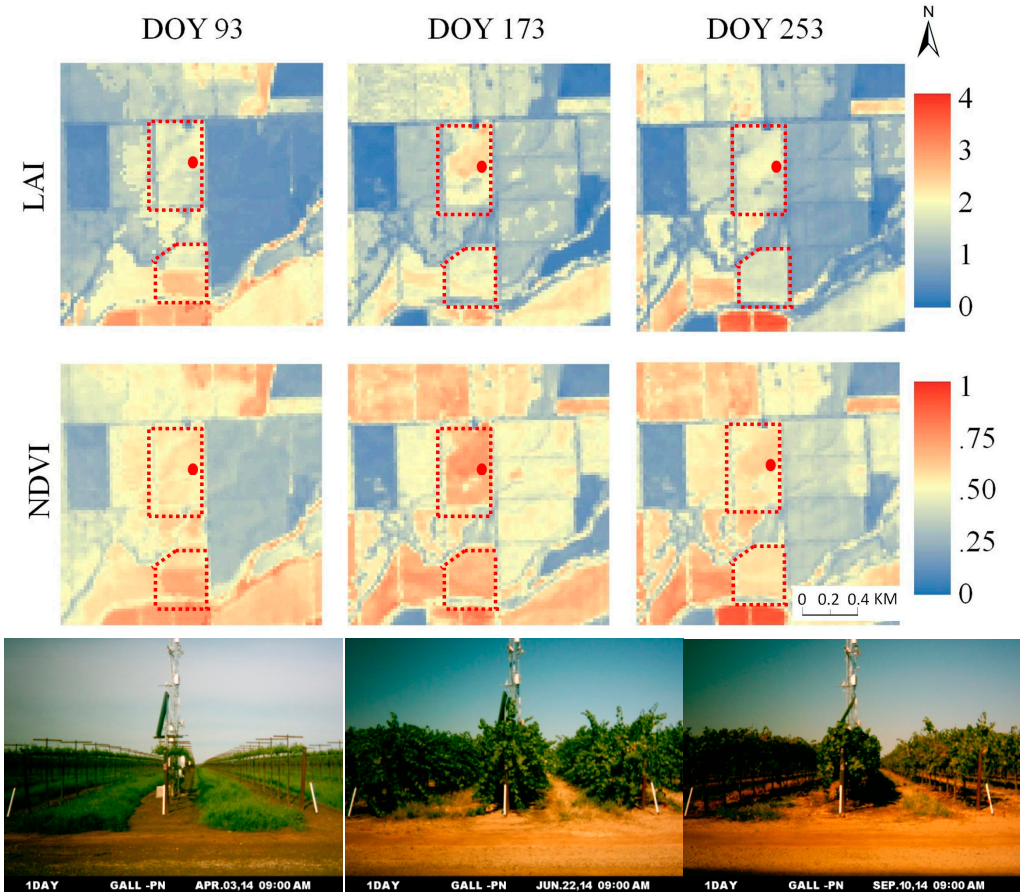

Figure 3. Landsat NDVI and LAI maps, and ground pictures on the three selected dates in 2014. (North and south field of GRAPEX vineyard are confined by dashed red line. Camera site is located in the north field and labeled as red dot).

The NDVI and LAI maps in Figure 3 also demonstrate within field spatial variation in vine development over the sampling area. The central part of the northern field shows higher LAI and NDVI, indicating a region of more vigorous vine growth. Lower LAI and NDVI in the upper left of the northern field are associated with soil texture discontinuities. The major soil type in the two fields is Kimball silt loam but there are small areas within the field (such as in the upper left corner of the northern field) with silt loam and gravelly loam soils which have poor to moderate water storage capacity [22]. The area of low LAI and NDVI at the top middle of the northern field is associated with a house, parking area, and storage sheds where equipment is kept for maintaining the fields.

NDVI and LAI averaged values (3 × 3 pixels) extracted from the sampling locations at Sites 1 and 2 (indicated in Figure 1) are shown in Figure 4. NDVI and LAI derived from L8 SR data are greater than those from L7, especially in the middle of the season where the difference is up to about 0.1 for NDVI and 0.5–1 for LAI. In addition, this difference is greater at Site 1 than at Site 2. Several studies have pointed out that surface reflectance differences between L7 and L8 result from quite different spectral response functions, resulting in higher values of NDVI from L8 than from L7 [40–42], which is consistent with our results. The reasons for these differences are complex, being dependent on the sensor differences in bands reflectance, view zenith angle, etc. [41], and will not be further explored in this study.

The GRAPEX study area is located within the overlap between adjacent WRS paths (43 and 44) and typically has low cloud cover during the grape growing season; therefore, there are sufficient Landsat 7 and 8 data available to provide a seasonable baseline, and then to form a smoothed growing curve using the Savitzky–Golay (SG) filtering algorithms from TIMESAT. The Landsat 7 ETM+ images

had less valid pixels due to the SLC failure especially in 2014. We used all valid pixels from Landsat 7 and 8. The original gaps in the Landsat 7 images were filled through the TIMESAT fitting process. In Figure 4, both NDVI and LAI show similar growth curves. The start of the growing season is around DOY 100 (middle of April), after which the leaf area increases quickly until the peak greenness period around DOY 150 (early of June). There is usually more than one peak in leaf biomass after DOY 150, especially for the south field inboth years. Although we do not have photos at Site 2 from 2013 and 2014 to examine the field conditions, it could be the result of pruning followed by vine re-growth which serves to shade the ripening grapes in the late summer from too much radiation. Overall, the LAI continues to decrease after DOY 150, and the end of the growing season is around DOY 250 (early September).

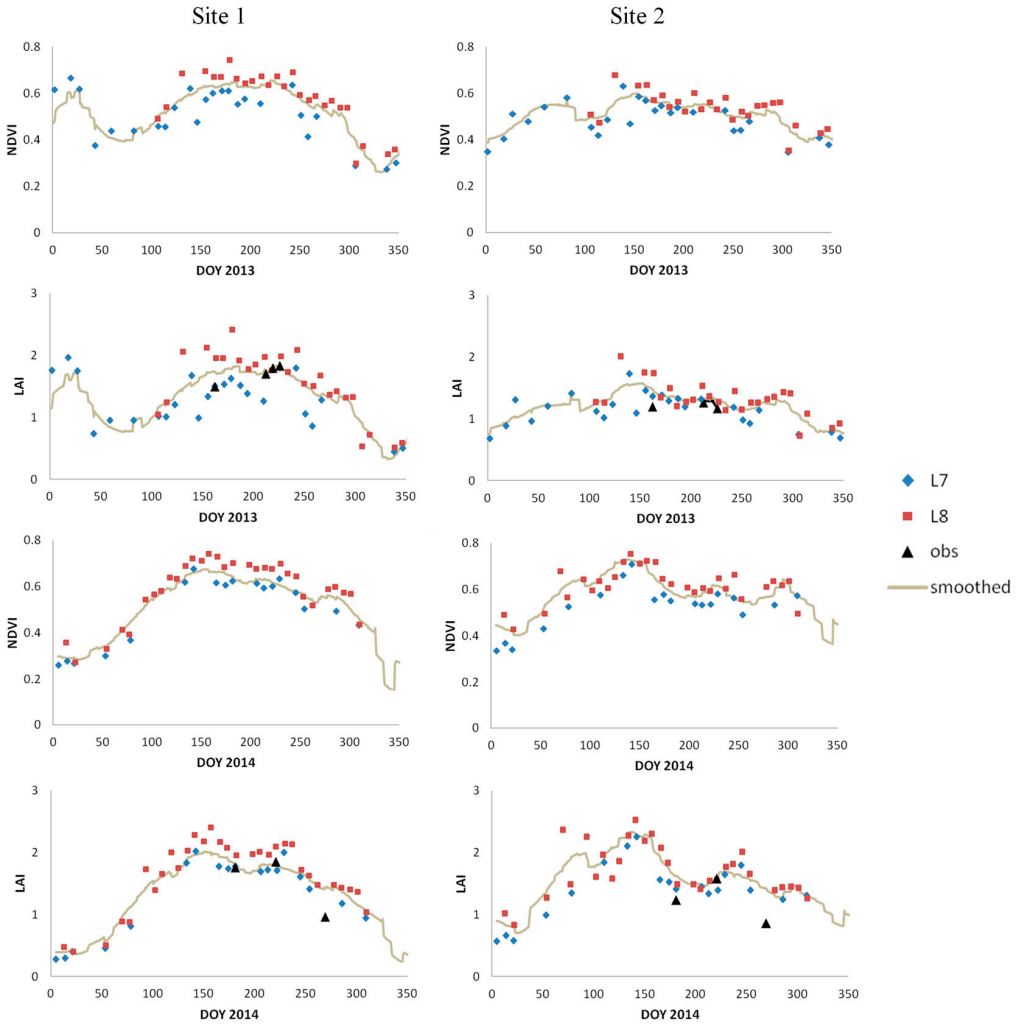

Figure 4. Landsat NDVI, LAI and ground measured LAI for both sites in 2013 and 2014.

Observed values of LAI, collected in-field, are also included in Figure 4. In general, the observed LAI is in good agreement with the smoothed growing curves formed by TIMESAT, except the measurement on DOY 269 of 2014. Although there is no valid estimated Landsat LAI on DOY 269 of 2014, Landsat LAI from both DOY 262 and 278 is 1.4–1.5, which is higher than the observed LAI on DOY 269 (0.96 for north site and 0.86 for south site). The leaves during this period had obviously started to senesce compared to peak conditions, meanwhile the grass cover crop is significant which is reflected on the Landsat pixels. However, the observed LAI measured with the Li-Cor LAI-2200 on DOY 269 did not include the grass cover crop resulting in lower observed LAI.

4.2. Spatial Correlation between Yield and Daily NDVI and LAI

The daily NDVI and LAI images were used to compute spatial correlations with yield maps collected for the north and south vineyards in 2013 and 2014. Correlation coefficients are shown in Figure 5 as a function of day of VI retrieval. The R curves for NDVI and LAI have similar trends in all cases except for the south field for 2014, as discussed below. The growing season started later in 2013 than in 2014, so from DOY 91 to DOY 110 of 2013 the correlation of both NDVI and LAI is strongly affected by the grass cover crop resulting in poor correlations with grape yield in this period. In 2013, the NDVI and LAI correlation curve for both vineyards are similar, increasing to 0.8 in the early growing season (in early May as the grass cover crop senesced), then decreasing to 0.6 (north vineyard) and 0.4 (south vineyard) by the end of the growing season. Figure 6 shows the yield maps for 2013 and the evolution of LAI from DOY 110–140, during the period of maximum yield correlation, which occurred around DOY 140 for the north field and DOY 130 for the south field. From DOY 110–140, the LAI spatial pattern became more and more like the yield spatial pattern. This seems very early in the season to have the highest correlation with yield, which may be due to the management of the vineyard later in the season.

In 2014, high winter (especially February–March) temperatures and faster accumulation of growing degree days led to an early start of season. In the north vineyard (Figure 5c), yield–NDVI/LAI correlations increase quickly from DOY 91 (R = 0) to DOY 110 (about R = 0.5), then more slowly to about 0.7 at the end of growing season. The south vineyard (Figure 5d) exhibits a very different correlation behavior, with negative correlations (R = −0.5) at DOY 130, and a peak positive correlation of R = 0.5–0.6 around DOY 180. The negative correlations early in the season relate to patterns in the development and management of the cover crop in the south vineyard. As apparent in Figure 7, the grass LAI was higher in the northern part of that field—opposite to trends in grape production. It is clear that NDVI/LAI-based predictions of yield variability should be limited to the period of vine growth, where vine LAI dominates the surface reflectance signal.

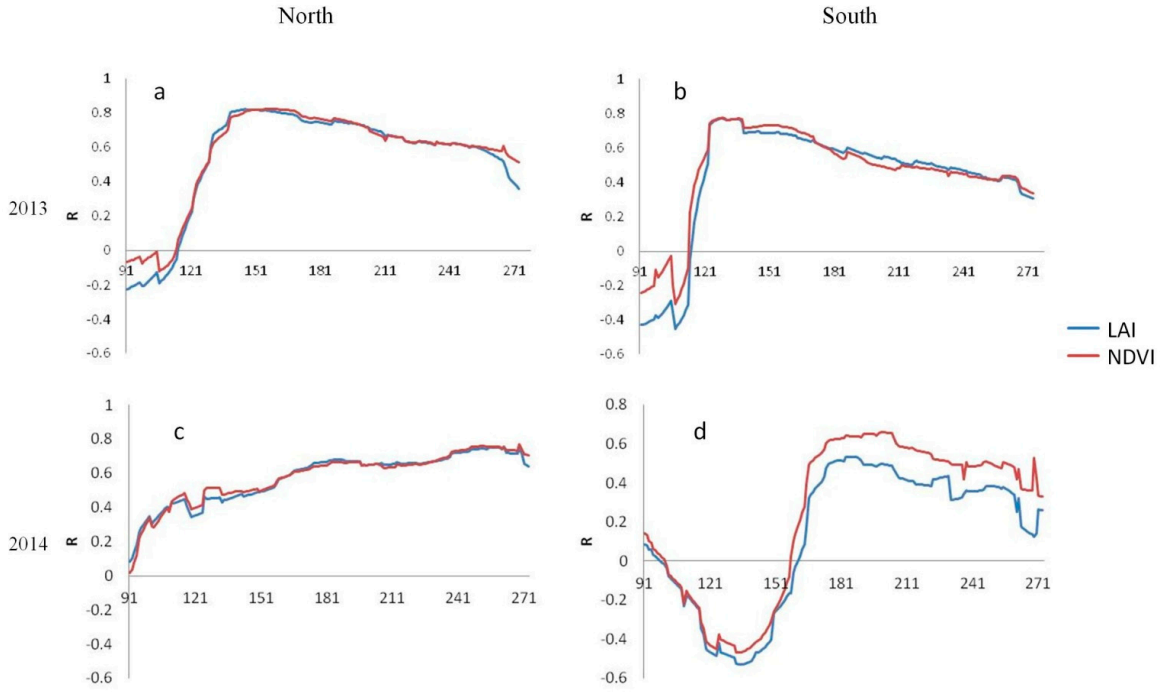

Figure 5. Spatial correlation coefficients (R) between yield and the smoothed daily NDVI/LAI (solid lines in Figure 4) in 2013 (**a**,**b**) and 2014 (**c**,**d**) using all pixels in the north (**a**,**c**) and south (**b**,**d**) vineyard.

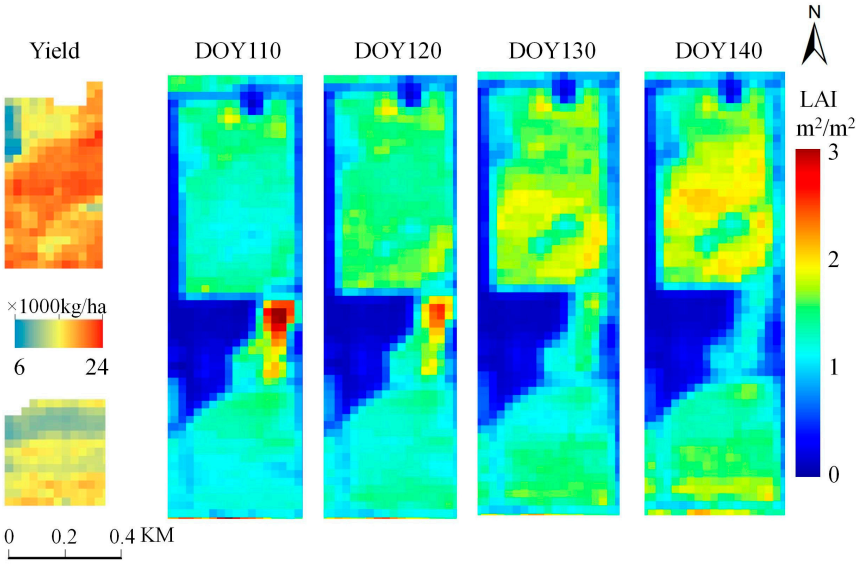

Figure 6. Yield maps for 2013 along with Landsat LAI retrievals for DOY 110–140.

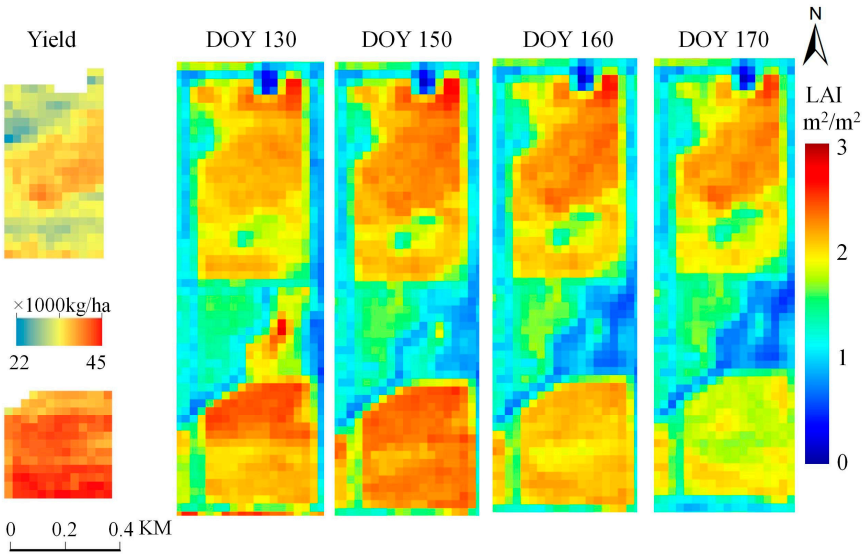

Figure 7. Yield maps for 2014 along with Landsat LAI retrievals for DOY 130–170.

While LAI and NDVI have similar performance in terms of yield correlations in most cases, Figure 5 shows that NDVI correlations are higher for the southern field in 2014. The spatial distribution for both indices is similar during the period of peak correlation, but with a slightly higher level of noise/speckle in LAI likely due to artifacts in the MODIS downscaling. In general, NDVI may be a smoother and more reliable indicator of yield in vineyards, which are not likely to suffer from significant saturation effects due to the strong row structure.

4.3. Optimal Temporal Window for Yield Prediction Using NDVI and LAI Timeseries

To better identify the temporal window during which NDVI and LAI are most predictive of grape yields in this study, 2-D correlations plots are shown in Figure 8, computed between yields and indices averaged over windows ranging from one-day to 120-days (y-axis), with the window end date varying over the growing season (x-axis). Correlation strength is summarized by color, with red tones indicating index average windows with stronger correlations. The positive slope of the contour of

maximum correlation indicates that longer averaging windows are accompanied by a delay in the peak correlation signal. In general, there will be a tradeoff between early notification and confidence in yield forecasts [43]. In addition, we found that the highest correlation with yields for both NDVI and LAI for both fields and both years came from 1-day interval. The best correlation information statistics are summarized in Table 2. Sibley et al. [25] also found that when predicting maize yield, only using the vegetation index from a single date performed better than the method using two to four dates per season. However, Esquerdo et al. [44] found that a full-season averaging window was optimal for estimating soybean yields in Brazil using NDVI. Mkhabela et al. [45] found the best time for making an accurate maize yield forecast was from the late January through late March depending on the agro-ecological region. Anderson et al. [43] analyzed the relationship between remotely sensed indices and crop yield in Brazil and also found that in some regions, some degree of additional time-averaging (moving upwards in the plots) helps to improve correlations with yields. The results from all these studies indicate that the time interval related to the best correlation depends not only on the crop type, but also on the climate/weather conditions and management practices. Regardless of this dispute, in this study, we find there is a strong relationship between grape yield and remotely sensed vegetation indices. The correlation between NDVI and yield ranged from 0.66 to 0.83, and for LAI the correlation with yield ranged from 0.53 to 0.82. The best correlation time is different for the north and south vineyard from two years due to different management and weather conditions early in the season. Irrigation start date and amount, as well as frequency and distribution throughout the season will have a significant impact on canopy and crop development. However, since the physical and chemical properties of the soil vary throughout the vineyard, the effect of any uniformly applied input will result in different spatial variability patterns. Canopy management practices, such as leafing and hedging, will also influence canopy density. Nonetheless, a high and stable correlation (greater than 0.6) over both years and fields was found over a common area between 25 June and 9 August.

Table 2. Date of optimal NDVI/LAI-yield correlation for the north and south vineyards.

Year	Vineyard	R		End Day	
		NDVI	LAI	NDVI	LAI
2013	North	0.83	0.82	155	145
2013	South	0.78	0.77	128	128
2014	North	0.77	0.76	268	261
2014	South	0.66	0.53	198	185

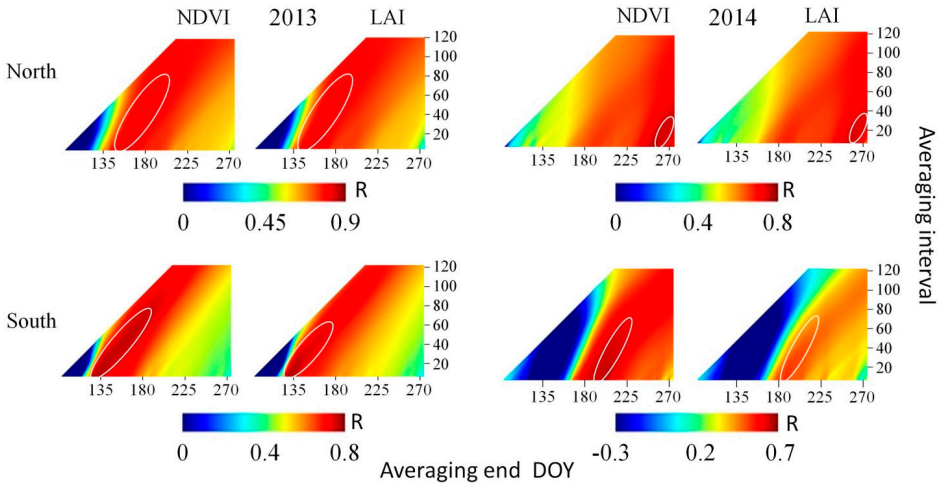

Figure 8. Correlation of yield with NDVI and LAI plotted as a function of index averaging interval (y-axis) and end date (x-axis). The peak correlation area is identified by a contour.

Figure 9 shows the scatter plots between NDVI and the yield on the best correlation date corresponding to Table 2. The yield range, especially for the south vineyard changed a lot between the two years, from 10–25 thousand kg/ha in 2013 to 30–50 in 2014. In addition, the slope of the fitting equation apparently increased in 2014 compared to that in 2013 for the both north and south vineyard, indicating that the yield variation became more sensitive to NDVI variation. In other words, the grape cluster density increased in 2014, which likely resulted from different management of the vineyard. However, the slope of the relationships for the north and south block is very close in the same year (66.8 and 60.6 in 2013, and 82 and 89.4 in 2014), indicating that the grape cluster density is similar in each year on both fields.

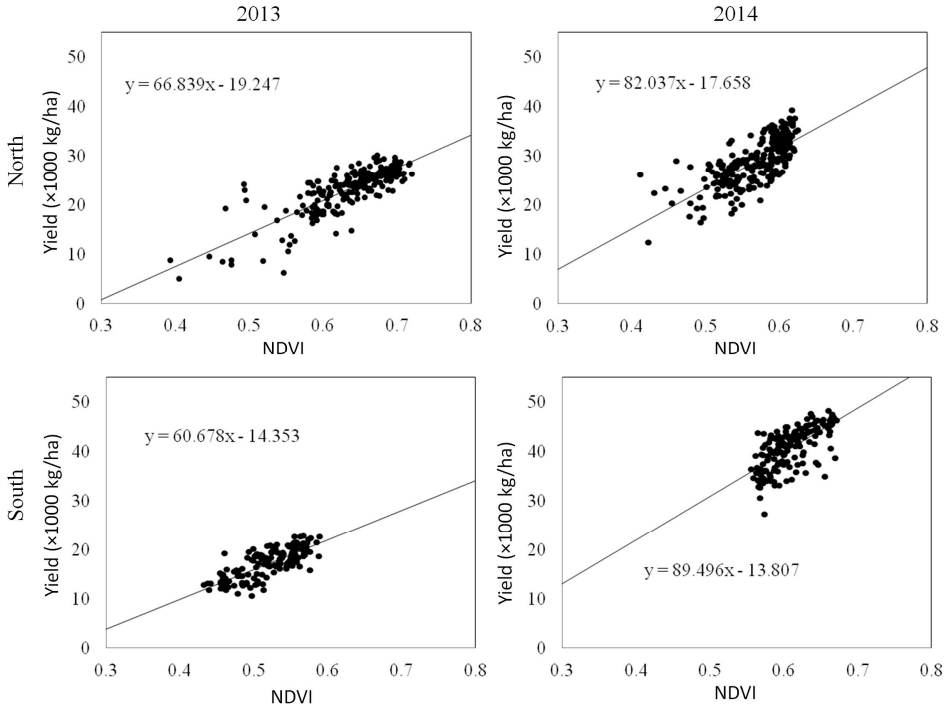

Figure 9. Scatter plots between NDVI and yield on the best correlation date identified in Table 2. The x-axis represents NDVI and the y-axis represents the yield (tons/acre). Fitting function labeled on each window.

4.4. A Simple Calibrated Method for Estimating Field-Scale Yield Variations

The varying slopes in NDVI vs. yield apparent in Figure 9 demonstrates the difficulties involved in using NDVI data alone to predict yield in wine grape vineyards. Management activities and variability in weather conditions interfere with natural relationships between leaf area and fruit production, and these management decisions are influenced by weather, disease, and also by economic and marketing factors that cannot be remotely-sensed. Still, there is the potential to combine remote sensing with standard field sampling that is already integral to the operational yield projection process which may significantly improve on current procedures and efficiently enhance the spatial detail of vineyard yield projections.

As a simple initial experiment, yields were sampled from the full maps at the points of minimum and maximum NDVI determined within a given field for a given year, as determined on the date of optimal correlation. This is analogous to targeted field sampling, using NDVI maps at critical growth stages to identify sampling points. Projected yield maps were then developed using a linear yield–NDVI function, scaled between these limits. Table 3 lists the prediction model coefficients and error statistics, showing low relative errors from 6.9–11.5%. The predicted and observed yield maps show similar spatial patterns (Figure 10), reflecting primarily variations in soil type and vine health.

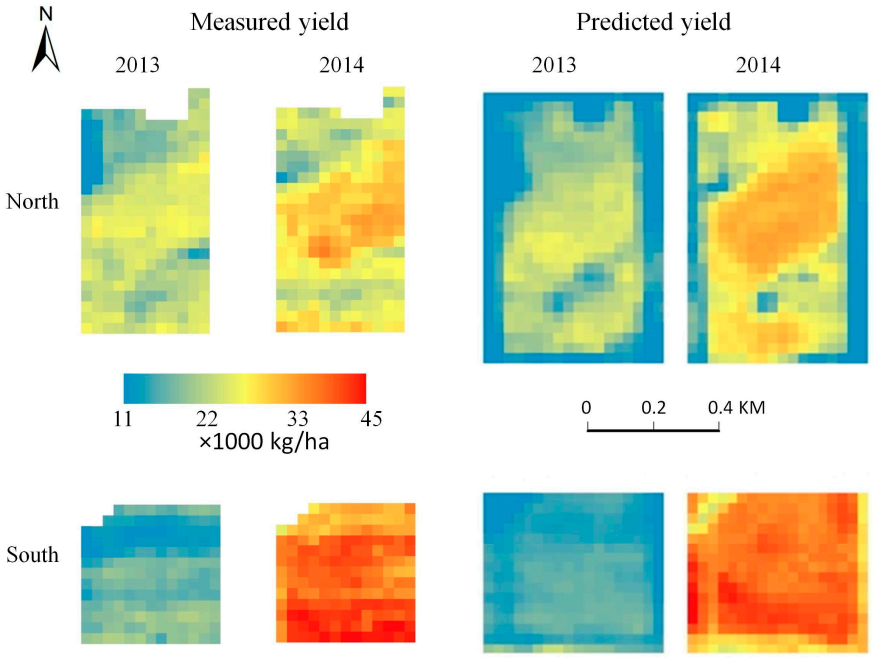

Figure 10. Grape yield maps for north and south field of 2013 and 2014.

Table 3. The prediction model coefficients (yield = a × NDVI + b) and error statistics.

Year	Vineyard	Coefficients of Prediction Function a/b	Bias ($\times 10^3$ kg/ha)	RMSE ($\times 10^3$ kg/ha)	Predicted Production ($\times 10^3$ kg)	Measured Production ($\times 10^3$ kg)	Relative Error (%)
2013	North	23.78/−5.41	−1.50	3.12	471	529	10.9
2013	South	28.07/−6.40	1.17	2.26	279	253	10.5
2014	North	19.16/3.73	3.88	5.25	749	653	14.8
2014	south	37.79/−4.76	0.20	3.12	635	600	5.9

In practice, however, the date of optimal correlation will not be known a priori and may vary from year to year. A more generalized summary of the NDVI data must be used. Therefore, the correlations between yield and maximum and cumulative indices during the growing season (over DOY 110 to 250) and during optimal common period in Section 4.4 (over DOY 151 to 221) were also evaluated and compared as shown in Table 4. Neither index combination is as good as the correlation from the best date. For the maximum index, the correlation of the south field in 2014 is negative, because the maximum index is mostly from DOY 140–150 and it is negatively correlated during this period for the south vineyard in 2014 (Figure 5). Thus, the two types of cumulative index (DOY 110–250 and DOY 151–221) are more stable than the maximum index. According to this comparison, another strategy was attempted to predict the grape yield based on the cumulative NDVI. The yield prediction relative errors range from 10 to 18%, which is, as expected, a little larger than that in Table 3, but it is still better than the industry performance of around 30% [46].

Table 4. Correlation between yield and maximum and cumulative indexes (NDVI and LAI) during the entire growing season (DOY 110 to 250) and the optimal period (DOY 156 to 221).

Year	Vineyard	R (Max Index)		R (Cum Entire)		R (Cum Optimal)	
		NDVI	LAI	NDVI	LAI	NDVI	LAI
2013	North	0.70	0.70	0.77	0.77	0.77	0.76
2013	South	0.70	0.58	0.68	0.67	0.62	0.63
2014	North	0.60	0.58	0.64	0.63	0.65	0.67
2014	South	−0.38	−0.44	0.45	0.21	0.63	0.48

5. Discussion

5.1. Importance of High Spatiotemporal Resolution Remote Sensing Data

At the Landsat scale (30 m), phenology and water use can be differentiated by crop type and land management practice [47], making this an optimal scale for assessments of crop yield, water productivity, and moisture conditions [48–50]. In this study, Landsat enabled us to investigate and analyze variations in vegetation conditions at sub-field scales. Meanwhile, the crop conditions changed quickly in critical growing stages even during a short time period as shown in Figure 5, which required a continuous timeseries of satellite data. To highlight this point, two pictures taken from the north vineyard during the rapid development stage (9 and 12 May 2013) are shown in Figure 11. Even though these are only three days apart, the leaf density of the vines on 12 May is obviously larger than that on 9 May (readers can compare the right row on the picture).

Figure 11. Vine growing conditions on 9 and 12 May 2013 over the north vineyard.

There are enough clear Landsat overpass images available in this study area to generate the timeseries NDVI/LAI. In other regions with higher frequency of cloud cover, data fusion methodologies, combining the high spatial resolution of Landsat with the daily temporal frequency of MODIS or similar moderate resolution systems, facilitates estimation of daily vegetation indices or evapotranspiration at sub-field scales [22,23,51]. In addition, medium resolution data from Sentinel-2A or other sensors can also be incorporated for monitoring crop conditions at field scale using a data normalization approach [52].

Unlike cereals, vineyards are not continuous crop, which means the ground information from the inter-row other than the vine canopy would be captured by Landsat images as mixed pixels. The effect of grass cover crop could be seen from NDVI/LAI maps on DOY 93 in Figure 3. However, based on the investigation of ground pictures and communication with growers, the grass cover crop had little impact on NDVI/LAI estimation during June and August which is the critical growth stage. As described in Section 3.1, the grass cover crop flourishes in very early season and become senescent in early May. From the correlation curve of 2013 in Figure 5 we can see that this is the period (after DOY 120) when the correlation between NDVI/LAI and yield started to increase, indicating that the grass cover crop had less and less impact. The research here presented that 30 m resolution Landsat images have the ability to evaluate variation in vine conditions. Certainly, very high resolution images with meter-level resolution will help us to better understand the vineyard conditions, especially the inter-row ground information. GRAPEX was designed to collect very high resolution (2 m) images vineyards from an airborne platform at critical growth stages. Combining continuous Landsat 30 m data and 2 m airborne information would be useful for vineyard management.

5.2. Grape Yield Prediction

It has been found that there are significant correlations between NDVI and vine canopy vigor [7], and it is possible to develop a relationship between NDVI and grape yield [53]. However, wine grape yield prediction is always a challenge not only because of climate factors, but also the trade-off between yield and quality [3], which means maximizing yield is not the only purpose of wine grape growers, but also market demand and quality have to be considered. In this case, there are many vineyard management techniques in the growing season that can affect yields. In the study of Cunha et al. [6], the relationship between NDVI and wine grape yield was significantly negative, explained by excessive vegetation growth of grapevines with dense canopies can causing shading and low bud fruitfulness [54]. However, the relationship is positively correlated in this study, indicating that the relationship between remotely sensed vegetation indices and wine grape yield has different performance under different environmental conditions and management strategies. Meanwhile, Cunha et al. [6] found that NDVI during the middle of April of the previous season (initiation of inflorescence) showed the best correlation with wine grape yield and this relationship is stable and consistent over the vineyard in Portugal. However, in our study, the best relationship only exists in 2013 for both the north and south field, but not for 2014. This may result from management effects in 2014, which is also confirmed by the unusual spatial pattern change over the south vineyard in 2014 (Figure 7), which had much greater yield, even greater than the north vineyard.

Accordingly, it is very difficult to predict the best correlation day and then to find a universal grape yield prediction model based on remotely sensed data. Therefore, in this study, we evaluated the relationship between yield and different NDVI/LAI combinations and found that although cumulative NDVI/LAI is not as good as the NDVI/LAI from the optimal date, it is better than the maximum NDVI/LAI and more stable across both years and both vineyards. Thus cumulative NDVI/LAI is possible to use for yield prediction in practice. Moreover, the finding of a common period of strong correlation across both vineyards and both years should be analyzed using more data from 2015 and 2016, which may be a better solution for yield prediction. The simple grape yield prediction strategy proposed in this study is based on the inner-annual NDVI/LAI combination before harvest, which demonstrates potential for practical application in the future.

Grape yield and quality is also associated with water stress [55]. Monitoring vineyard water use and improving water management are important purpose of GRAPEX. Preliminary results about spatio-temporal continuous 30 m resolution evapotranspiration (ET) maps of 2013 generated by a multi-satellite fusion program has been evaluated over GRAPEX vineyards, and the ET maps shows general spatial correspondence with yield maps [22]. Therefore, in the next study, further insightsand improved grape yield prediction strategies could be expected by combining high spatio-temporal resolution NDVI/LAI and ET maps.

6. Conclusions

High temporal-spatial resolution remote sensing vegetation index data or imagery is critical to monitor field scale crop conditions. In this study, Landsat reflectance products from 2013 and 2014 were acquired over two vineyards in California, USA. Daily 30 m resolution NDVI and LAI was interpolated using adaptive Savitzky–Golay filtering function supplied by TIMESAT. The results showed that spatial variability of yield can be described by remote sensing data. There is apparently a correlation in the temporal variation curve for both the north and south vineyards and the best correlation (0.66–0.83) shows a specific time which is inconsistent for the two years evaluated in this study. The relationship between yield and maximum and cumulative index (NDVI and LAI) was also investigated. The correlation with yield for the cumulative index (0.64–0.74, except south vineyard in 2014) is better than the maximum index (0.6–0.7, except the south vineyard in 2014), and both are not as good as the index from the best correlation date. These remote sensing metrics could be used for grape yield prediction calibration using a few ground measurements with relative error of less than 20%. This can improve yield estimation and reduce time from traditional grape yield estimation

approaches. To determine the optimal dates for grape yield predicting for the region, more vineyards in the region need to be included and analyzed using the same approach. In addition, inter-annual variability of yield is more complex and influenced by management practices in addition to other factors including weather.

Acknowledgments: This work was partially supported by the NASA Science of Terra and Aqua program (NNH13ZDA001N-TERAQ), the NASA Applied Sciences Program and the US Geological Survey (USGS) Landsat Science Team program. The collection of field data was funded in part by E. & J. Gallo Winery. In addition, we would like to thank the staff of Viticulture, Chemistry and Enology Division of E. & J. Gallo Winery, in particular Nick Dokoozlian Vice President, who supported the field data collection and made possible access to the vineyard sites for the GRAPEX project. USDA is an equal opportunity provider and employer.

Author Contributions: William P. Kustas, Martha C. Anderson, Luis Sanchez and Brent Sams conceived and designed the experiments; Lynn McKee, Wayne Dulaney, Maria M. Alsina and William A. White performed the experiments; Joseph G. Alfieri and John H. Prueger collected the data; Forrest Melton and Kirk Post mounted the camera and provided images; Feng Gao proposed the idea and provide the method; Liang Sun analyzed the data and wrote the paper; and Martha C. Anderson helped to improve the manuscript.

Conflicts of Interest: The authors declare no conflict of interest.

References

1. California Department of Food and Agriculture, & U.N. A.S. S. California Grape Acreage Report 2015. Available online: https://www.nass.usda.gov/Statistics_by_State/California/Publications/Fruits_and_Nuts/2016/201604grpac.pd (accessed on 19 April 2016).
2. Clingeleffer, P. Crop Development, Crop Estimation and Crop Control to Secure Quality and Production of Major Wine Grape Varieties: A National Approach. Available online: http://research.wineaustralia.com/wp-content/uploads/2012/09/CSH-96-1.pdf (accessed on 11 Octorber 2016).
3. Sabbatini, P.; Dami, I.; Howell, G.S. Predicting Harvest Yield in Juice and Wine Grape Vineyards. Available online: http://msue.anr.msu.edu/uploads/resources/pdfs/Predicting_Harvest_Yield_in_Juice_and_Wine_Grape_Vineyards_%28E3186%29.pdf (accessed on 19 April 2016).
4. Wolpert, J.A.; Vilas, E.P. Estimating Vineyard Yields: Introduction to a Simple, Two-Step Method. *Am. J. Enol. Vitic.* **1992**, *43*, 384–388.
5. Tarara, J.M.; Chaves, B.; Sanchez, L.A.; Dokoozlian, N.K. Analytical determination of the lag phase in grapes by remote measurement of trellis tension. *HortScience* **2013**, *48*, 453–461.
6. Cunha, M.; Marçal, A.R.S.; Silva, L. Very early prediction of wine yield based on satellite data from VEGETATION. *Int. J. Remote Sens.* **2010**, *31*, 3125–3142. [CrossRef]
7. Johnson, L.F.; Roczen, D.E.; Youkhana, S.K.; Nemani, R.R.; Bosch, D.F. Mapping vineyard leaf area with multispectral satellite imagery. *Comput. Electron. Agric.* **2003**, *38*, 33–44. [CrossRef]
8. Hall, A.; Lamb, D.W.; Holzapfel, B.; Louis, J. Optical remote sensing applications in viticulture—A review. *Aust. J. Grape Wine Res.* **2002**, *8*, 36–47. [CrossRef]
9. Hall, A.; Louis, J.; Lamb, D. A Method For Extracting Detailed Information From High Resolution Multispectral Images of Vineyards. In Proceedings of the 6th International Conference on Geocomputation, Brisbane, Australia, 24–26 September 2001.
10. Lamb, D.; Weedon, M.M.; Bramley, R.G.V. Using remote sensing to predict grape phenolics and colour at harvest in a Cabernet Sauvignon vineyard: Timing observations against vine phenology and optimising image resolution image. *Aust. J. Grape Wine Res.* **2004**, *10*, 46–54. [CrossRef]
11. Brady, J.; Wiley, S. Tading AIMS amongst the vines. *Aust. Grapegrow. Winemak.* **2000**, *441*, 73–75.
12. Arkun, S.; Dunk, I.J.; Ranson, S.M. Hyperspectral remote sening for vineyard management. In Proceedings of the 1st National Conference on Geospatial Information & Agriculture, Sydney, Australia, 6 July 2001; pp. 586–599.
13. Myneni, R.B.; Hoffman, S.; Knyazikhin, Y.; Privette, J.L.; Glassy, J.; Tian, Y.; Wang, Y.; Song, X.; Zhang, Y.; Smith, G.R.; et al. Global products of vegetation leaf area and fraction absorbed PAR from year one of MODIS data. *Remote Sens. Environ.* **2002**, *83*, 214–231. [CrossRef]
14. Anderson, M.C.; Neale, C.M.U.; Li, F.; Norman, J.M.; Kustas, W.P.; Jayanthi, H.; Chavez, J. Upscaling ground observations of vegetation water content, canopy height, and leaf area index during SMEX02 using aircraft and Landsat imagery. *Remote Sens. Environ.* **2004**, *92*, 447–464. [CrossRef]

15. Dong, T.; Liu, J.; Qian, B.; Zhao, T.; Jing, Q.; Geng, X.; Wang, J.; Huffman, T.; Shang, J. Estimating winter wheat biomass by assimilating leaf area index derived from fusion of Landsat-8 and MODIS data. *Int. J. Appl. Earth Obs. Geoinf.* **2016**, *49*, 63–74. [CrossRef]
16. Huang, J.; Tian, L.; Liang, S.; Ma, H.; Becker-Reshef, I.; Huang, Y.; Su, W.; Zhang, X.; Zhu, D.; Wu, W. Improving winter wheat yield estimation by assimilation of the leaf area index from Landsat TM and MODIS data into the WOFOST model. *Agric. For. Meteorol.* **2015**, *204*, 106–121. [CrossRef]
17. Ganguly, S.; Nemani, R.R.; Zhang, G.; Hashimoto, H.; Milesi, C.; Michaelis, A.; Wang, W.; Votava, P.; Samanta, A.; Melton, F.; et al. Generating global Leaf Area Index from Landsat: Algorithm formulation and demonstration. *Remote Sens. Environ.* **2012**, *122*, 185–202. [CrossRef]
18. Fang, H.L.; Liang, S.L. Retrieving leaf area index with a neural network method: Simulation and validation. *IEEE Trans. Geosci. Remote Sens.* **2003**, *41*, 2052–2062. [CrossRef]
19. Gobron, N.; Pinty, B.; Verstraete, M.M. Theoretical limits to the estimation of the leaf area index on the basis of visible and near-infrared remote sensing data. *IEEE Trans. Geosci. Remote Sens.* **1997**, *35*, 1438–1445. [CrossRef]
20. Gao, F.; Anderson, M.C.; Kustas, W.P.; Wang, Y. Simple method for retrieving leaf area index from Landsat using MODIS leaf area index products as reference. *J. Appl. Remote Sens.* **2012**, *6*, 063554.
21. Anderson, M.C.; Kustas, W.P.; Norman, J.M.; Hain, C.R.; Mecikalski, J.R.; Schultz, L.; González-Dugo, M.P.; Cammalleri, C.; D'Urso, G.; Pimstein, A.; et al. Mapping daily evapotranspiration at field to continental scales using geostationary and polar orbiting satellite imagery. *Hydrol. Earth Syst. Sci.* **2011**, *15*, 223–239. [CrossRef]
22. Semmens, K.A.; Anderson, M.C.; Kustas, W.P.; Gao, F.; Alfieri, J.G.; McKee, L.; Prueger, J.H.; Hain, C.R.; Cammalleri, C.; Yang, Y.; et al. Monitoring daily evapotranspiration over two California vineyards using Landsat 8 in a multi-sensor data fusion approach. *Remote Sens. Environ.* **2016**, *185*, 155–170. [CrossRef]
23. Cammalleri, C.; Anderson, M.C.; Gao, F.; Hain, C.R.; Kustas, W.P. Mapping daily evapotranspiration at field scales over rainfed and irrigated agricultural areas using remote sensing data fusion. *Agric. For. Meteorol.* **2014**, *186*, 1–11. [CrossRef]
24. Cammalleri, C.; Anderson, M.C.; Gao, F.; Hain, C.R.; Kustas, W.P. A data fusion approach for mapping daily evapotranspiration at field scale. *Water Resour. Res.* **2013**, *49*, 4672–4686. [CrossRef]
25. Sibley, A.M.; Grassini, P.; Thomas, N.E.; Cassman, K.G.; Lobell, D.B. Testing Remote Sensing Approaches for Assessing Yield Variability among Maize Fields. *Agron. J.* **2014**, *106*, 24. [CrossRef]
26. Sakamoto, T.; Gitelson, A.A.; Arkebauer, T.J. MODIS-based corn grain yield estimation model incorporating crop phenology information. *Remote Sens. Environ.* **2013**, *131*, 215–231. [CrossRef]
27. Lobell, D.B.; Thau, D.; Seifert, C.; Engle, E.; Little, B. A scalable satellite-based crop yield mapper. *Remote Sens. Environ.* **2015**, *164*, 324–333. [CrossRef]
28. Steduto, P.; Hsiao, T.C.; Fereres, E.; Raes, D. Crop yield response to water. FAO Irrigation and Drainage Paper 66. Available online: http://www.fao.org/docrep/016/i2800e/i2800e00.htm (accessed on 19 April 2016).
29. Guérif, M.; Duke, C.L. Adjustment procedures of a crop model to the site specific characteristics of soil and crop using remote sensing data assimilation. *Agric. Ecosyst. Environ.* **2000**, *81*, 57–69. [CrossRef]
30. Garrigues, S.; Lacaze, R.; Baret, F.; Morisette, J.T.; Weiss, M.; Nickeson, J.E.; Fernandes, R.; Plummer, S.; Shabanov, N.V.; Myneni, R.B.; et al. Validation and intercomparison of global Leaf Area Index products derived from remote sensing data. *J. Geophys. Res.* **2008**, *113*, G02028. [CrossRef]
31. Yang, W.; Shabanov, N.V.; Huang, D.; Wang, W.; Dickinson, R.E.; Nemani, R.R.; Knyazikhin, Y.; Myneni, R.B. Analysis of leaf area index products from combination of MODIS Terra and Aqua data. *Remote Sens. Environ.* **2006**, *104*, 297–312. [CrossRef]
32. Jönsson, P.; Eklundh, L. TIMESAT—A program for analyzing time-series of satellite sensor data. *Comput. Geosci.* **2004**, *30*, 833–845. [CrossRef]
33. Jonsson, P.; Eklundh, L. Seasonality extraction by function fitting to time-series of satellite sensor data. *IEEE Trans. Geosci. Remote Sens.* **2002**, *40*, 1824–1832. [CrossRef]
34. Heumann, B.W.; Seaquist, J.W.; Eklundh, L.; Jönsson, P. AVHRR derived phenological change in the Sahel and Soudan, Africa, 1982–2005. *Remote Sens. Environ.* **2007**, *108*, 385–392. [CrossRef]
35. Gao, F.; Morisette, J.T.; Wolfe, R.E.; Ederer, G.; Pedelty, J.; Masuoka, E.; Myneni, R.; Tan, B.; Nightingale, J. An algorithm to produce temporally and spatially continuous MODIS-LAI time series. *IEEE Geosci. Remote Sens. Lett.* **2008**, *5*, 60–64. [CrossRef]

36. Zhang, X.; Friedl, M.A.; Schaaf, C.B.; Strahler, A.H.; Hodges, J.C.F.; Gao, F.; Reed, B.C.; Huete, A. Monitoring vegetation phenology using MODIS. *Remote Sens. Environ.* **2003**, *84*, 471–475. [CrossRef]
37. Hird, J.N.; McDermid, G.J. Noise reduction of NDVI time series: An empirical comparison of selected techniques. *Remote Sens. Environ.* **2009**, *113*, 248–258. [CrossRef]
38. Xia, T.; Kustas, W.P.; Anderson, M.C.; Alfieri, J.G.; Gao, F.; McKee, L.; Prueger, J.H.; Geli, H.M.E.; Neale, C.M.U.; Sanchez, L.; et al. Mapping evapotranspiration with high resolution aircraft imagery over vineyards using one and two source modeling schemes. *Hydrol. Earth Syst. Sci. Discuss.* **2016**, *12*, 11905–11957. [CrossRef]
39. USGS Home. Available online: http://earthexplorer.usgs.gov/ (accessed on 19 April 2016).
40. Holden, C.E.; Woodcock, C.E. An analysis of Landsat 7 and Landsat 8 underflight data and the implications for time series investigations. *Remote Sens. Environ.* **2015**, *185*, 16–36. [CrossRef]
41. Roy, D.P.; Kovalskyy, V.; Zhang, H.K.; Vermote, E.F.; Yan, L.; Kumar, S.S.; Egorov, A. Characterization of Landsat-7 to Landsat-8 reflective wavelength and normalized difference vegetation index continuity. *Remote Sens. Environ.* **2016**, *185*, 57–70. [CrossRef]
42. Ke, Y.; Im, J.; Lee, J.; Gong, H.; Ryu, Y. Characteristics of Landsat 8 OLI-derived NDVI by comparison with multiple satellite sensors and in-situ observations. *Remote Sens. Environ.* **2015**, *164*, 298–313. [CrossRef]
43. Anderson, M.C.; Zolin, C.A.; Sentelhas, P.C.; Hain, C.R.; Semmens, K.; Tugrul Yilmaz, M.; Gao, F.; Otkin, J.A.; Tetrault, R. The Evaporative Stress Index as an indicator of agricultural drought in Brazil: An assessment based on crop yield impacts. *Remote Sens. Environ.* **2016**, *174*, 82–99. [CrossRef]
44. Esquerdo, J.C.D.M.; Zullo Júnior, J.; Antunes, J.F.G. Use of NDVI/AVHRR time-series profiles for soybean crop monitoring in Brazil. *Int. J. Remote Sens.* **2011**, *32*, 3711–3727. [CrossRef]
45. Mkhabela, M.S.; Mkhabela, M.S.; Mashinini, N.N. Early maize yield forecasting in the four agro-ecological regions of Swaziland using NDVI data derived from NOAA's-AVHRR. *Agric. For. Meteorol.* **2005**, *129*, 1–9. [CrossRef]
46. Dunn, G. Yield Forecasting. Available online: http://gwrdc.com.au/wp-content/uploads/2012/09/2010-06-FS-Yield-Forecasting.pdf (accessed on 19 April 2016).
47. Anderson, M.C.; Allen, R.G.; Morse, A.; Kustas, W.P. Use of Landsat thermal imagery in monitoring evapotranspiration and managing water resources. *Remote Sens. Environ.* **2012**, *122*, 50–65. [CrossRef]
48. Jiang, Z.; Chen, Z.; Chen, J.; Liu, J.; Ren, J.; Li, Z.; Sun, L.; Li, H. Application of Crop Model Data Assimilation With a Particle Filter for Estimating Regional Winter Wheat Yields. *IEEE J. Sel. Top. Appl. Earth Obs. Remote Sens.* **2014**, *7*, 4422–4431. [CrossRef]
49. Sun, L.; Sun, R.; Li, X.; Liang, S.; Zhang, R. Monitoring surface soil moisture status based on remotely sensed surface temperature and vegetation index information. *Agric. For. Meteorol.* **2012**, *166–167*, 175–187. [CrossRef]
50. Sun, L.; Liang, S.; Yuan, W.; Chen, Z. Improving a Penman–Monteith evapotranspiration model by incorporating soil moisture control on soil evaporation in semiarid areas. *Int. J. Digit. Earth* **2013**, *6*, 134–156. [CrossRef]
51. Gao, F.; Masek, J.; Schwaller, M.; Hall, F. On the blending of the landsat and MODIS surface reflectance: Predicting daily landsat surface reflectance. *IEEE Trans. Geosci. Remote Sens.* **2006**, *44*, 2207–2218.
52. Gao, F.; Masek, J.G.; Wolfe, R.E.; Huang, C. Building a consistent medium resolution satellite data set using moderate resolution imaging spectroradiometer products as reference. *J. Appl. Remote Sens.* **2010**, *4*, 043526.
53. Lamb, D.; Hall, A.; Louis, J. Airborne remote sensing of vines for canopy variability and productivity. *Aust. Grapegrow. Winemak.* **2001**, *449*, 89–92.
54. Sánchez, L.A.; Dokoozlian, N.K. Bud Microclimate and Fruitfulness in *Vitis vinifera* L. *Am. J. Enol. Vitic.* **2005**, *56*, 319–329.
55. Chaves, M.M.; Santos, T.P.; Souza, C.R.; Ortuño, M.F.; Rodrigues, M.L.; Lopes, C.M.; Maroco, J.P.; Pereira, J.S. Deficit irrigation in grapevine improves water-use efficiency while controlling vigour and production quality. *Ann. Appl. Biol.* **2007**, *150*, 237–252. [CrossRef]